THE JOURNAL OF PHYSICAL CHEMISTRY B

Article

pubs.acs.org/JPCB

Monte Carlo Simulation for the Double Layer Structure of an Ionic Liquid Using a Dimer Model: A Comparison with the Density Functional Theory

Lutful Bari Bhuiyan,*[,†] Stanisław Lamperski,*[,‡] Jianzhong Wu,*[,§] and Douglas Henderson*[,∥]

[†]Laboratory of Theoretical Physics, Department of Physics, University of Puerto Rico, Rio Piedras, Puerto Rico 00936-8377

[‡]Department of Physical Chemistry, Adam Mickiewicz University, Grunwaldzka 6, 60-780 Poznań, Poland

[§]Department of Chemical and Environmental Engineering, University of California, Riverside, California 92521-0425, United States

[∥]Department of Chemistry and Biochemistry, Brigham Young University, Provo, Utah 84602-5700, United States

ABSTRACT: Theoretical difficulties in describing the structure and thermodynamics of an ionic liquid double layer are often associated with the nonspherical shapes of ionic particles and extremely strong electrostatic interactions. The recent density functional theory predictions for the electrochemical properties of the double layer formed by a model ionic liquid wherein each cation is represented by two touching hard spheres, one positively charged and the other neutral, and each anion by a negatively charged hard spherical particle, remain untested in this strong coupling regime. We report results from a Monte Carlo simulation of this system. Because for an ionic liquid the Bjerrum length is exceedingly large, it is difficult to perform simulations under conditions of strong electrostatic coupling used in the previous density functional theory study. Results are obtained for a somewhat smaller (but still large) Bjerrum length so that reliable simulation data can be generated for a useful test of the corresponding theoretical predictions. On the whole, the density profiles predicted by the theory are quite good in comparison with the simulation data. The strong oscillations of ionic density profiles and the local electrostatic potential predicted by this theory are confirmed by simulation, although for a small electrode charge and strong electrostatic coupling, the theory predicts the contact ionic densities to be noticeably different from the Monte Carlo results. The theoretical results for the more important electrostatic potential profile at contact are given with good accuracy.

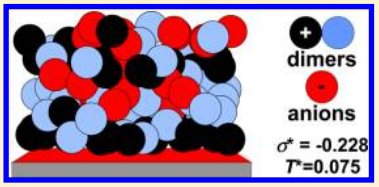

1. INTRODUCTION

Most theoretical studies of the double layer formed by ions near a charged electrode are based on models that employ charged hard spheres to represent ionic species. The solvent is typically replaced by a dielectic continuum whose relative permittivity is equal to that of the pure solvent. This model is called the primitive model (PM) or, in the case of hard spheres that are of the same size, the restricted primitive model (RPM). The use of a dielectric continuum for the solvent simplifies the theoretical analysis substantially but confuses the comparison with the experimental analysis because the contribution of the solvent (usually water) is put into empirically adjusted parameters that describe what is often called the compact layer. In essence, the discreteness of the solvent and the ensuing solvent structure are neglected. Indeed, the few studies that use molecular models of the solvent do indicate that the interfacial layer of the solvent is not compact but is as diffuse as the interfacial layer of the ions.[1] This is reasonable since the interfacial bare electric field is damped by the ion charges, and hence, a field will exist over the entire diffuse layer. Thus, as long as there is an interfacial electric field, the solvent molecules will be influenced by this field; the interfacial solvent layer must be as thick as the interfacial diffuse ionic layer. As a result, simple theories based on the primitive model may be useful for correlating experimental data but can give an incomplete picture of the structure of the double layer at a molecular level.

Electric double layers are commonplace in industrial applications.[2] Recent years have seen a renewed interest in studies of double layers containing ionic liquids, in part due to the broad applications of such liquids, which are essentially room temperature molten salts. Ionic liquids are environmentally friendly solvents useful in separation processes and portable energy devices such as supercapacitors and lithium-ion batteries. Because they exist as liquid at room temperature, ionic liquids are more suitable for experimental study than molten salts. Typically, molten salts melt at a temperature of thousands of degrees, and great care must be employed by an experimentalist while studying them. Because there is no solvent, experimental results from an ionic liquid may provide better insight into the structure of an electric double layer. The temptation to lump everything not understood into a parametrized compact layer is absent. However, to use a cliché, there is no free lunch. The main difficulties, in theory at least, with the use of ionic liquids in theoretical investigations are, first, the ions are usually not spheres and, second, because there is no solvent with a large dielectric constant to reduce the electrostatic interactions, the electrostatic coupling, as defined

Received: May 5, 2012
Revised: July 3, 2012
Published: August 3, 2012

dx.doi.org/10.1021/jp304362y | J. Phys. Chem. B 2012, 116, 10364−10370

by the Bjerrum length, can be almost 2 orders of magnitude greater than that of an aqueous electrolyte.

From an experimental point of view, although direct information about the structure of the interfacial ionic liquid double layer through diffraction probes remains technically elusive, indirect structural information through measurements of, for example, double layer thickness, capacitance, and surface electrochemical characteristics is widely available. We refer the reader to recent reviews by Aliaga et al.[3] and Salminem et al.[4] A parallel account of theoretical progress in capacitance calculations has been outlined by Kornyshev.[2]

Theoretical studies of ionic liquid double layers have tended to fall into two classes. One approach is to assume that the ions are approximately spherical. The early simulation study of Boda and Henderson[5] is an example of this class. More recent studies using spherical ions include those of Lamperski et al.,[6−8] Loth et al.,[9] and some of us.[10] Modeling ions as charged hard spheres has the advantage that most existing double layer theories can be used. However, the problem is that spherical particles may be an extreme simplification for the geometry of cations or anions in an ionic liquid. Another approach is to pick a specific ionic liquid and use as realistic a model as possible. Such realistic ionic models can be studied by means of a simulation,[11−13] but there is little hope for a sophisticated theory for a complex model. Moreover, the results obtained will tend to be specific to the system considered. In contrast, a simple generic model that uses nonspherical ions, but is simple enough for theoretical study, may give general insights into ionic liquid double layers and consequently can be more useful. One promising system is a model ionic liquid in which one ion is a dimer consisting of two touching hard spheres, one of which is charged and the other neutral; a second ion is a rigid charged sphere, of the opposite sign, to complete global electrostatic neutrality. The assignment of specific charges to the dimer and the sphere is unimportant since reversing the electrode charge gives the other case. This system has been studied by Fedorov et al.[14] and some of us[10,15] using the density functional theory (DFT). This dimer model represents the alkyl cation of some ionic liquids and has been used by Fedorov et al. It has also been used to model tetraethylammonium in a study of an ionic liquid in a pore.[16] Of course, the dimer does not model all ionic liquids, but in simulating a molecule with an off-center charge, it introduces asymmetry and is, thus, a step beyond the spherical ions used in many previous studies. We have found the DFT robust enough to give promising results, and it is to be hoped, accurate, at conditions of strong electrostatic coupling that are inherent to ionic liquids.

However, this hope for accuracy must be tested. Simulation results are used as a benchmark against which a theory is assessed. Molecular simulation provides data that are, apart from statistical considerations, numerically reliable; the statistical uncertainty can be minimized through long simulation runs. As long as the theory and simulation use the same molecular model and interaction potentials, the corresponding simulation data provide a means by which the theoretical predictions can be calibrated. In this study, we use the Monte Carlo (MC) simulation to test the numerical performance of the DFT for double layers of ionic liquids. Because reliable MC results were not attained in a reasonable period of computational time for the ionic liquid model, MC simulation was performed for a system that had a Bjerrum length that is 10 times greater than that of an aqueous system at room temperature. In an ionic liquid that is free of solvent, electrostatic interactions are about 80 times greater than those in the aqueous system. Boda et al.[5] had this same difficulty in their simulations of molten salt double layers. We note that Fedorov et al. also made their simulations at a smaller coupling constant (or, equivalently, at a higher temperature) than that of their model. Perhaps a smaller Bjerrum length is appropriate, due to the presence of interactions that result in a residual dielectric constant that is greater than unity and/or the sphere diameters that are greater than those considered in our DFT study. Very likely, hard spheres are an oversimplification for ionic particles; including a soft repulsion and an attractive dispersion force might help. Nonetheless, we believe a comparison of DFT with simulation results at conditions of strong electrostatic coupling will be useful and informative even if it is not as large as those used in our DFT study.[10] In this work, we performed MC simulations using the same molecular parameters as before[10,15] and with as strong an electrostatic coupling as would still yield convergence in a reasonable period of simulation time. Since the dimer model could also be used for a double layer consisting of a nonspherical aqueous electrolyte, we also report some results for this dimer system with a Bjerrum length appropriate for an aqueous system. In order to focus on the effect of the electrostatic coupling on the double layer structure, we report results for the aqueous system at the high density level of an ionic liquid. In later work, we will examine the double layer of the dimer system for couplings and concentrations appropriate for electrolyte solutions.

2. MODEL

In our simulation and DFT calculations, the interaction between hard spheres of species i and j, whose centers are separated by distance r, is given by

$$\beta u_{ij}(r) = \begin{cases} \infty, & r < d \\ Z_i Z_j l_B / r, & r > d \end{cases} \quad (1)$$

where $\beta = 1/(k_B T)$ with k_B and T being the Boltzmann constant and the absolute temperature, respectively. The hard core ($r < d$) represents the short-range repulsions that mimic the Pauli exclusion principle. The parameter $l_B = \beta e^2/4\pi\varepsilon_0\varepsilon_r$ stands for the Bjerrum length, where e is the magnitude of the elementary charge, ε_0 is the permittivity of free space, and ε_r is the relative permittivity of the solvent. The parameter d is the diameter of the hard spheres, which is taken to be equal for all the spheres. We use d = 4.25 Å, as this value is often used in molecular simulations. The valences, Z_i, are +1 and 0 for the two spheres in the dimer cation and −1 for the spherical anion. A pair of positive and neutral spheres is tethered to form a dimer of touching spheres. This assignment of positive and negative valences is only for definiteness as we report results for both positive and negative electrode charges. The charges of the spheres are assumed to be located at their centers. In our previous DFT work, the Bjerrum length was l_B = 556.92 Å, a value that corresponds to electrostatic interaction in a vacuum (ε_r = 1) at 298.15 K. As we have mentioned, it is difficult to obtain convergence with such a large value of l_B. Here we used l_B = 56.7 Å, which was about the largest value of l_B for which we could obtain sensible results in a reasonable simulation time. Additionally in the development of our simulation code, we used l_B = 7.14 Å, which corresponds to that for an aqueous solution at room temperature. We report simulation and DFT

dx.doi.org/10.1021/jp304362y | J. Phys. Chem. B 2012, 116, 10364−10370

results for both values of l_B in order to see the effect of electrostatic coupling.

The interaction of a sphere with the electrode is given by

$$\beta W_i(x) = \begin{cases} \infty, & x < d/2 \\ -(2\pi l_B Z_i \sigma/e)x, & x > d/2 \end{cases} \quad (2)$$

where x is the perpendicular distance of the center of the sphere from the electrode surface. The parameter σ denotes the surface charge density of the electrode, which is assumed to be planar, smooth, and nonpolarizable. The electrode charge is located on the surface, that is, zero skin depth. The electrode is assumed to have the same dielectric constant as the electrolyte.

The structure of the interface is described by the density profiles of the ions, $\rho_i(x)$, which give the local number densities of the ions of species i as a function of the perpendicular distance x from the electrode surface. We report results for the normalized density profiles, $g_i(x) = \rho_i(x)/\rho_i(\infty)$. Once the density profiles are determined, the mean electrostatic potential profile is calculated from

$$\psi(x) = \frac{e}{\varepsilon_0} \sum_i Z_i \int_x^\infty dx'(x - x')\rho_i(x') \quad (3)$$

and the charge density of the interface is given by

$$\sigma = -e \sum_i Z_i \int_{d/2}^\infty dx' \rho_i(x') \quad (4)$$

These expressions result from the integration of Gauss' law at a planar hard surface, using the boundary conditions of vanishing field and potential at an infinite distance from the electrode. In the DFT calculations, the density profiles and the local electrostatic potential are determined simultaneously. Because of electrostatic neutrality, the charge density of the interface must be equal in magnitude, but opposite in sign, to the integrated charge density of the mobile ions. Otherwise, there would be an electric field infinitely far from the electrode. The values of $\rho_i(x)$ are such that $\rho_i(\infty) = \rho_i$, where ρ_i is simply the bulk number density of ions of species i.

We use dimensionless units throughout this work, namely, $\sigma^* = \sigma d^2/e$, $\psi^*(x) = \beta e \psi(x)$, $\rho_i^*(x) = \rho_i(x)d^3$, and the reduced temperature, $T^* = d/l_B$. The bulk density of the spherical ions, and of the charged and neutral spheres of the dimers, is taken to be $\rho_i^* = 0.15$. This density is appropriate for an ionic liquid. The total reduced density of all the spheres is 0.45.

The system is at room temperature (T = 298.15 K), but for an ionic liquid, T^* is very small because $\varepsilon_r = 1$ in the absence of a solvent. The values of T^* that correspond to l_B = 556.92 and 56.7 Å are 0.00763 and 0.075, respectively. The value of T^* for an aqueous electrolyte at room temperature is 0.595, which corresponds to l_B = 7.14 Å. We report simulation results for this reduced temperature to gain insight into the effect of changes in the reduced temperature. The value of ρ_i^* used here is too large for an aqueous electrolyte. Later, we will report results for T^* = 0.595 at densities appropriate for such systems, in order to analyze the effects of ionic shape on the electrochemical properties of an ordinary electrolyte solution.

3. THEORY AND SIMULATION METHOD

We used both DFT and MC simulations to calculate the density and the mean electrostatic potential profiles. The detailed equations for the DFT and its numerical implementation have been reported in previous publications[15,16] and will not be repeated here. The MC simulations were performed in the canonical (NVT) ensemble using the standard Metropolis algorithm. The simulation cell was a rectangular parallelepiped of dimensions $X \times Y \times Z$ with $Y = Z$. The two opposite sides, viz., the yz planes at $x = 0$ and $x = X$, respectively, across the longer edge X were the two hard walls of which the wall at $x = 0$ was the electrode with a uniformly charged surface, while the other at $x = X$ was uncharged. A dimer was formed by attaching a neutral hard sphere at a randomly chosen point on the surface of a positive ion so that the dimer length (defined as the separation between the centers of the two touching spheres) was equal to the common diameter d used for all of the particles. In all the calculations reported here, the dimer length was fixed. Besides the usual random movements of dimers and anions, we also considered rotation of the dimers following the techniques introduced by Allen and Tildsley.[17] We examined both positive and negative surface charge densities on the electrode. The surface charge density σ was calculated from the difference between the number of dimer cations, N_+, and the number of spherical anions, N_-, present in the cell.

$$\sigma = -\frac{e(Z_-N_- + Z_+N_+)}{Y^2} \quad (5)$$

The negative sign on the right-hand side of the equation occurs because the entire system satisfies electrostatic neutrality. For example, for the 1:1 valency systems considered here, if $N_- > N_+$, the surface charge density is positive. Similarly, a negative surface charge on the electrode was obtained by choosing $N_- < N_+$. We used the conventional minimum image method together with periodic boundary conditions along the y and z directions parallel to the walls.[17] The long-range aspect of the Coulomb interactions was treated by the charged sheets method of Torrie and Valleau,[18] which has since been improved upon by Boda et al.[19] A trial-and-error adjustment of the MC cell length, X, was required to achieve the given bulk concentration. The total number of particles (all ions and the neutral spheres) used in a simulation varied typically between 800 and 900, while microscopic configurations on the order of 7×10^8 were generated of which the first 2×10^8 were used to equilibrate the system, with the remaining ones being used in the calculations for the average density profiles $\rho_i(x)$. These densities were used to calculate the local electric potential profile $\psi(x)$ using eq 3. To ensure confidence in the simulation results, two independent codes were written in Pascal and Fortran. This is not an insignificant difference because it requires a different structure for each code. Additionally, the codes were run on different machines. The accepted results were those that fell within the statistical uncertainties of each other.

4. RESULTS

In Figures 1−6, we report results for the reduced mean electrostatic potential profile, $\psi^*(x)$, and the normalized density profiles, $g_i(x)$, for appreciable positive and negative values of the electrode charge, σ^*, and zero electrode charge for both T^* = 0.595 and 0.075. As indicated earlier, all calculations were done at ρ_i^* = 0.15. The DFT density profiles for the higher reduced temperature, shown in Figures 1−3, are in very good agreement with the MC results. Both the density and the potential profiles oscillate at such high densities as one would expect. For T^* = 0.595 and a positive electrode charge (Figure

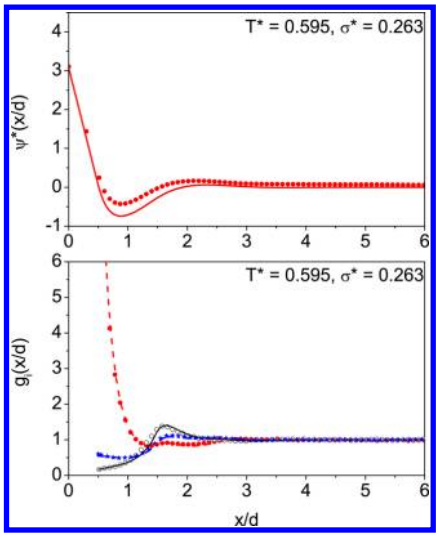

Figure 1. Dimensionless potential, $\psi^*(x)$, and reduced density profiles, $g_i(x)$, as a function of the dimensionless normal distance from the electrode, x/d, for $T^* = 0.595$, $\sigma^* = 0.263$, and $\rho_i^* = 0.15$. On the top, the lines give the DFT results, and the filled circles give the MC results for the potential. On the bottom, the lines and symbols give the DFT and MC results, respectively, for $g_i(x)$. The solid (black) line and the open circles give the DFT and MC results, respectively, for the positively charged dimer sphere; the dash-dot (blue) line and stars give the DFT and MC results, respectively, for the neutral dimer sphere, and the dashed (red) line and filled circles give the DFT and MC results for the negatively charged spheres, respectively.

1), the negative spheres are attracted to the electrode, while the positive ends of the dimers are, in general, repelled. Some of the neutral ends manage to be near the electrode. However, farther from the electrode, the positive and neutral ends of the dimer both have a peak at $x/d \sim 1.6$, suggesting a parallel orientation. Charge inversion, which is also seen in double layers of spherical ions, occurs in the vicinity of the peak of the dimer profile. For this same large value of T^*, but for a negative electrode charge (Figure 2), the positive ends of the dimers are

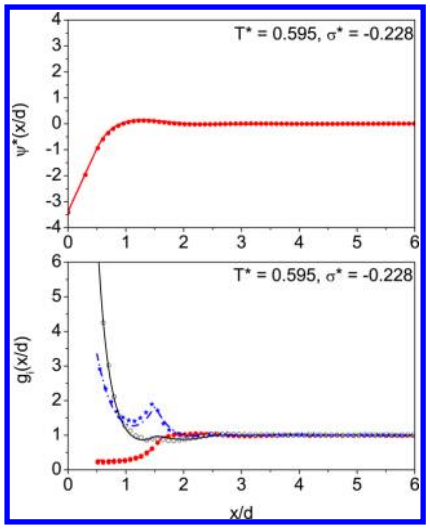

Figure 2. Dimensionless mean electrostatic potential, $\psi^*(x)$, and reduced density profiles, $g_i(x)$, as a function of the dimensionless normal distance from the electrode, x/d, for $T^* = 0.595$, $\sigma^* = -0.228$, and $\rho_i^* = 0.15$. The symbols and lines have the same meaning as in Figure 1.

attracted to the electrode, and the neutral ends of the dimer are dragged along. Near the electrode, the negative ions are repelled. There is a peak in the profile of the neutral dimer spheres at about $x/d \sim 1.5$, indicating a roughly perpendicular orientation of many of the dimers near the electrode. However, again some neutral ends manage to be near the electrode, so some parallel orientations occur in this region. Charge inversion is weak for this case. For this higher value of T^*, the positive, neutral, and negative spheres are all found near the uncharged electrode (Figure 3), although the charges of the

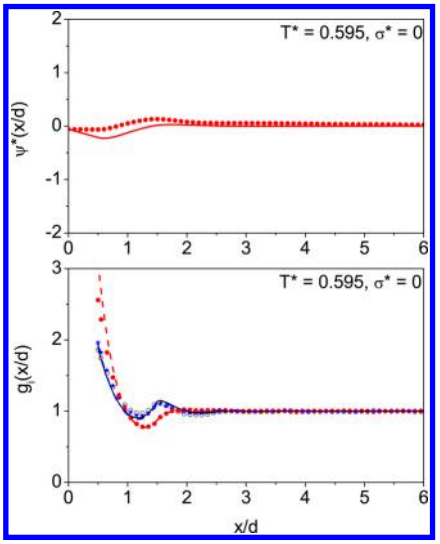

Figure 3. Dimensionless mean electrostatic potential, $\psi^*(x)$, and reduced density profiles, $g_i(x)$, as a function of the dimensionless normal distance from the electrode, x/d, for $T^* = 0.595$, $\sigma^* = 0$, and $\rho_i^* = 0.15$. The symbols and lines have the same meaning as in Figure 1.

negative spheres seems to predominate near the electrode. The dimers near the electrode tend to be oriented parallel to the electrode. Charge inversion does occur for an uncharged electrode, with the positive charge being relatively more prevalent further from the electrode. The DFT $\psi^*(x)$ results are in good overall agreement with those of the MC. Some differences appear near $x = d$ for the positive and zero charge cases. However, the DFT contact potential, $\psi(0)$, is very accurate. This is important because $\psi(0)$ yields the capacitance.

Results for $T^* = 0.075$ are displayed in Figures 4–7. Although some inaccuracy in the DFT values of the potential profile is apparent, the theory again predicts good results for the important value, $\psi^*(0)$. The oscillations in the density profiles are more pronounced for the smaller value of T^*. As expected, the negative spheres predominate near a positively charged electrode (Figure 4). The DFT prediction for the density profile of the negative spheres, $\rho_-(x)$, is quite accurate. The number of neutral dimer ends near a positive electrode is slightly overestimated by the DFT. The positive and neutral dimer spheres dominate roughly around $x \sim 1.5d$, suggesting the prevalence of a parallel dimer orientation. Charge inversion is apparent with further layering observed at greater distances. For the negatively charged electrode (Figure 5), the positive ends of the dimers are attracted. The presence of some neutral dimer ends suggests partial parallel orientations, but the broad peaks further out indicate that roughly perpendicular orientations are more prevalent. In the case of the uncharged electrode (Figure 6), the DFT profiles show appreciable

dx.doi.org/10.1021/jp304362y | J. Phys. Chem. B 2012, 116, 10364–10370

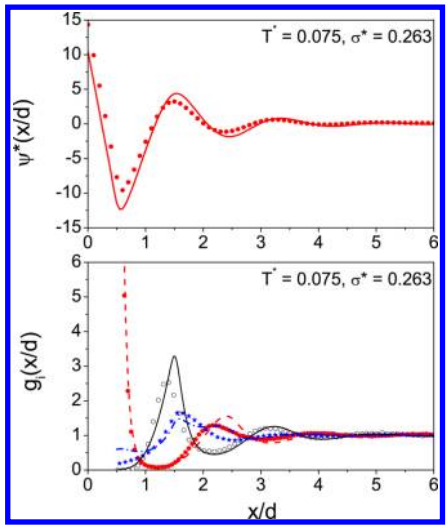

Figure 4. Dimensionless mean electrostatic potential, $\psi^*(x)$, and reduced density profiles, $g_i(x)$, as a function of the dimensionless normal distance from the electrode, x/d, for $T^* = 0.075$, $\sigma^* = 0.263$, and $\rho_i^* = 0.15$. The symbols and lines have the same meaning as in Figure 1.

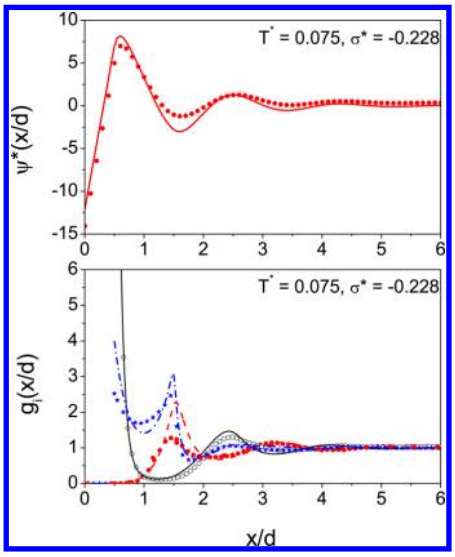

Figure 5. Dimensionless mean electrostatic potential, $\psi^*(x)$, and reduced density profiles, $g_i(x)$, as a function of the dimensionless normal distance from the electrode, x/d, for $T^* = 0.075$, $\sigma^* = -0.228$, and $\rho_i^* = 0.15$. The symbols and lines have the same meaning as in Figure 1.

deviations, but this does not affect the important value of $\psi(0)$. The significant difference is most likely due to the use of the mean-spherical approximation (MSA) for the direct correlation functions of the bulk electrolyte but probably also, in part, due to the use of a different independent variable (electrode potential vs electrode charge) in the DFT and MC calculations. Because of strong electrostatic interactions and relatively weak inhomogeneity near a neutral surface, the difference between the MC and DFT can be easily magnified by even a small difference in the boundary conditions. In the MC profiles, the neutral dimer ends dominate near the electrode. The presence of a peak in the profile for the positive dimer spheres suggests a perpendicular orientation near the neutral electrode. Layering and charge inversion are also apparent. Despite a neutral

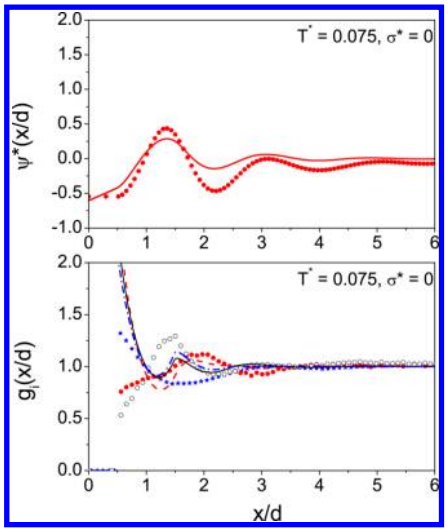

Figure 6. Dimensionless mean electrostatic potential, $\psi^*(x)$, and reduced density profiles, $g_i(x)$, as a function of the dimensionless normal distance from the electrode, x/d, for $T^* = 0.075$, $\sigma^* = 0$, and $\rho_i^* = 0.15$. The symbols and lines have the same meaning as in Figure 1.

surface that has no selectivity on the ionic species, inclusion of a neutral segment in each cation breaks the electrostatic symmetric thus leading to substantial segregation of the ionic density profiles. As is seen in Figure 6, zero electrode charge does not correspond to zero electrode potential. Further, the MC potential profile in Figure 6 shows substantial oscillations. Snapshots of typical dimer and spherical ion configurations at $T^* = 0.075$ for different values of σ^* are displayed in Figure 7.

The DFT values for $\psi^*(0)$ as a function of σ^* are plotted in Figure 8. The value of $\psi^*(0)$ decreases appreciably as T^* increases. However, the qualitative behavior of the $\psi^*(0)$ does not change. The differential capacitance has a parabolic shape at both values of T^*. Since the qualitative behavior is unchanged, the differential capacitance is not displayed.

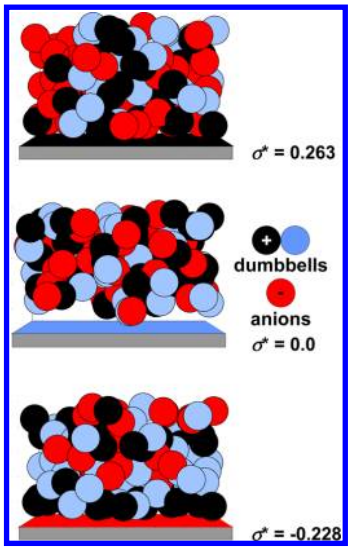

Figure 7. Snapshots of typical ionic configurations at $T^* = 0.075$ and $\rho_i^* = 0.15$ for the three values of σ^* considered in this work. The color scheme is the same as that of the other figures. The black and blue spheres are, respectively, the positive and neutral ends of the dimers, and the red spheres are the anions.

dx.doi.org/10.1021/jp304362y | J. Phys. Chem. B 2012, 116, 10364−10370

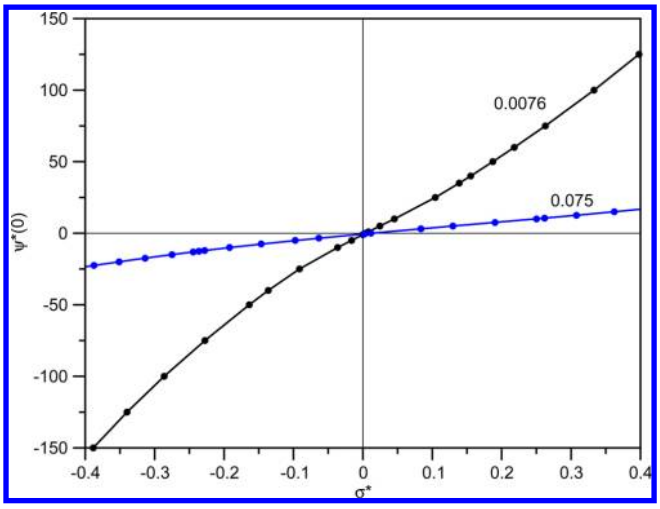

Figure 8. Dimensionless mean electrostatic potential at contact, $\psi^*(0)$, as a function of the reduced surface charge density σ^* for T^* = 0.0076 and 0.075. The points give the actual DFT results. The curves give the results obtained from a polynomial fit that was used to examine the differential capacitance.

5. CONCLUSION

The purpose of this study was 2-fold: to obtain, by means of MC simulation, "exact" structural results for a model ionic liquid double layer, and thereby test the accuracy of the DFT that has been reported recently.[15] Density functional and Monte Carlo results for an electrolyte consisting of negatively charged spheres and dimers composed of tethered spheres, one of which is positively charged with the other neutral, have been reported for a density appropriate for an ionic liquid. We considered a large reduced temperature, T^* = 0.595, that is appropriate for an aqueous electrolyte and a much smaller reduced temperature, T^* = 0.075. Our DFT gave good agreement with the MC results at the higher T^*. At the lower temperature, DFT gave good results for the density profiles of ionic species near a charged electrode. However, the density profiles showed significant deviations for the uncharged electrode, but this does not have much effect on the potential profile, especially at contact. The DFT potential profiles, particularly at contact, were given with good accuracy.

The errors in the DFT density profiles near the electrode at small T^* are not surprising since similar errors are seen in the application of the DFT to the double layer of a RPM electrolyte. For an uncharged electrode, the contact value of the density profile of an RPM electrolyte is given by the osmotic pressure in the bulk, which is nearly zero at small T^*. Density functional theory uses the MSA to obtain an analytic expression for the free energy functional of charged hard spheres. The MSA contact value is related to the compressibility of an uncharged hard sphere fluid, which exceeds unity. Errors in the contact values disappear when the electrode is charged, and the electrostatic contributions become dominant. The value of the electrode potential, $\psi^*(0)$, for a specific value of the electrode charge, σ^*, decreases markedly as T^* increases. However, the qualitative behavior of the dependence of $\psi^*(0)$ on σ^* does not change. In particular, the capacitance has a bell or parabolic shape at both values of T^*.

A comment on the small values of T^* that we have considered is in order. For charged spheres of equal size (the RPM), the liquid–vapor coexistence critical point temperature, calculated from the MSA (energy equation route), is T_c^* = 0.0786.[20,21] The correct (MC) result should be somewhat smaller but is not likely to be as low as T_c^* = 0.008. An attractive dispersion force would increase the critical point temperature, but this point has not been examined. The phase diagram of the dimer fluid is not known. In any case, we would like the system to be below its critical point but away from the triple point. While the model system discussed in this paper could be thermodynamically unstable at small values of T^*, ionic liquids do exist. The dimer model of ionic fluids is a useful approximation; the DFT gives quantitative values, especially for the electrostatic potential at the electrode, and it is useful for the study of ionic liquids. Possibly, using a residual dielectric constant greater than unity and a larger value for d would raise the appropriate value of T^*. Including an attractive dispersion force might help but is probably not worth the effort since such a force is unlikely to affect electrostatic effects greatly. The same issue arises with the RPM, where this model has proven useful in regions outside the liquid state conditions.

AUTHOR INFORMATION

Corresponding Author

*L.B.B.: e-mail, beena@beena.cnnet.clu.edu. S.L.: e-mail, slamper@amu.edu.pl. J.W.: e-mail, jwu@engr.ucr.edu. D.H.: e-mail, doug@chem.byu.edu.

Notes

The authors declare no competing financial interest.

ACKNOWLEDGMENTS

This work is in part supported by the National Science Foundation (NSF-CBET-0852353), the U.S. Department of Energy (DE-FG02-06ER46296), and the Adam Mickiewicz University, Faculty of Chemistry.

REFERENCES

(1) Henderson, D.; Boda, D. *Phys. Chem. Chem. Phys.* **2009**, *11*, 3822–3830.
(2) Kornyshev, A. A. *J. Phys. Chem. B* **2007**, *111*, 5545–5557.
(3) Aliaga, C.; Santos, C. S.; Baldelli, S. *Phys. Chem. Chem. Phys.* **2007**, *9*, 3683–3700.
(4) Salminem, J.; Papaiconomou, N.; Anand Kumar, R.; Lee, J.-M.; Kerr, J.; Newman, J.; Prausnitz, J. M. *Fluid Phase Equilib.* **2007**, *261*, 421–426.
(5) Boda, D.; Henderson, D.; Chan, K.-Y. *J. Chem. Phys.* **1999**, *110*, 5346–5350.
(6) Lamperski, S.; Outhwaite, C. W.; Bhuiyan, L. B. *J. Phys. Chem. B* **2009**, *113*, 8925–8929.
(7) Lamperski, S.; Henderson, D. *Mol. Simul.* **2011**, *37*, 264–268.
(8) Outhwaite, C. W.; Lamperski, S.; Bhuiyan, L. B. *Mol. Phys.* **2011**, *109*, 21–26.
(9) Loth, M. S.; Skinner, B.; Shklovskii, B. I. *Phys. Rev. E* **2010**, *82* (056102), 016107.
(10) Wu, J.; Jaing, T.; Jiang, D.; Jin, Z.; Henderson, D. *Soft Matter* **2011**, *7*, 11222–11231.
(11) Canongia Lopes, J. N. A.; Padua, A. A. H. *J. Phys. Chem. B* **2006**, *110*, 3330–3335.
(12) Smith, G. D.; Borodin, O.; Li, L.; Kim, H.; Liu, Q.; Bara, J. E.; Gin, D. L.; Nobel, R. *Phys. Chem. Chem. Phys.* **2008**, *10*, 6301–6312.
(13) Smith, G. D.; Borodin, O.; Magda, J. J.; Boyd, R. H.; Wang, Y. S.; Bara, J. E.; Miller, S.; Gin, D. L.; Nobel, R. D. *Phys. Chem. Chem. Phys.* **2010**, *12*, 7064–7076.
(14) Fedorov, M. V.; Georgi, N.; Kornyshev, A. A. *Electrochem. Commun.* **2010**, *12*, 296–299.
(15) Henderson, D.; Lamperski, S.; Jin, Z.; Wu, J. *J. Phys. Chem. B* **2011**, *115*, 12911–12914.

(16) Jiang, D.; Jin, Z.; Henderson, D.; Wu, J. *J. Phys. Chem. Lett.* **2012**, *3*, 1727−1731.
(17) Allen, M. P.; Tildsley, D. J. *Computer Simulation of Liquids*; Oxford University Press Inc.: New York, 1989.
(18) Torrie, G. M.; Valleau, J. P. *J. Chem. Phys.* **1980**, *73*, 5807−5816.
(19) Boda, D.; Chan, K.-Y.; Henderson, D. *J. Chem. Phys.* **1998**, *109*, 7362−7371.
(20) Sabir, A. K.; Bhuiyan, L. B.; Outhwaite, C. W. *Mol. Phys.* **1998**, *93*, 405−409.
(21) González-Tovar, E. *Mol. Phys.* **1999**, *97*, 1203−1206.